Since a given trial structure of a crystal is characterized by fixed values of σ_1 and $\langle|\Delta\mathbf{r}|\rangle$, for the evaluation of $\bar{R}(F)$ from (12), σ_1 and $\langle|\Delta\mathbf{r}|\rangle$ are to be treated as fixed quantities. The integral on the right-hand side of (12) is to be evaluated numerically. For this the values of $R(y)$ are needed at discrete values of S. This can in turn be obtained by first calculating the relevant values of D from (16) and then by interpolation.

The overall value of the conventional R index based on intensities is defined by

$$\bar{R}(I)=\frac{\sum|I_N-I_P^c|}{\sum I_N}. \tag{20}$$

By following a procedure similar to that employed for $R(F)$ and using the known result that $\langle y_N^2\rangle=1$ it can be shown that

$$\bar{R}(I)=\frac{\int_0^{S_{max}} f^2(S)S^2R(z)\,dS}{\int_0^{S_{max}} f^2(S)S^2\,dS}, \tag{21}$$

where

$$R(z)=\langle|y_N^2-\sigma_1^2y_P^{c2}|\rangle=\int_0^1\int_0^1\left|\left(\frac{u}{1-u}\right)^2-\sigma_1^2\left(\frac{v}{1-v}\right)^2\right| \times P\left(\frac{u}{1-u},\frac{v}{1-v}\right)\frac{du\,dv}{(1-u)^2(1-v)^2}. \tag{22}$$

The procedure for the evaluation of $\bar{R}(I)$ for any given trial structure is similar to that discussed earlier for $\bar{R}(F)$.

3. Discussion of the theoretical results

The overall values of $R(F)$ and $R(I)$ as functions of σ_1^2 and $\langle|\Delta\mathbf{r}|\rangle$ (in Å) were evaluated by the procedure discussed in § 2 by taking f in (12) and (21) to be the scattering factor of the C atom. S_{max} in (12) and (21) is taken to be 0·6485 which is the maximum value of $(\sin\theta)/\lambda$ corresponding to Cu $K\alpha$ radiation. The results thus obtained for $\bar{R}(F)$ and $\bar{R}(I)$ are given in Tables 1 and 2 respectively for the centrosymmetric case, and in Tables 3 and 4 for the non-centrosymmetric case. Since a major portion of an organic or a biomolecule is composed of C atoms and since the scattering powers of O and N are comparable with C, these results could be expected to hold good for organic crystal structures. A study of these tables shows that $\bar{R}(I)$ would be preferable to $\bar{R}(F)$ particularly in the conventional refinement stage.

MNP thanks the University Grants Commission, New Delhi, India for financial assistance.

References

LUZZATI, V. (1952). *Acta Cryst.* **5**, 802–810.
SRINIVASAN, R. & PARTHASARATHY, S. (1976). *Some Statistical Applications in X-ray Crystallography*. Oxford: Pergamon Press.
SRINIVASAN, R., RAGHUPATHY SARMA, V. & RAMACHANDRAN, G. N. (1963). *Crystallography and Crystal Perfection*. London and New York: Academic Press.
SRINIVASAN, R. & RAMACHANDRAN, G. N. (1965). *Acta Cryst.* **19**, 1003–1007.
WILSON, A. J. C. (1949). *Acta Cryst.* **2**, 318–321.
WILSON, A. J. C. (1950). *Acta Cryst.* **3**, 397–398.
WILSON, A. J. C. (1969). *Acta Cryst.* B**25**, 1288–1293.

Acta Cryst. (1979). A**35**, 675–684

Thermal Diffuse Scattering for Molecular Crystals: Errors in X-ray Diffraction Intensities and Atomic Parameters

BY P. A. KROON AND AAFJE VOS

Laboratorium voor Chemische Fysica, Rijksuniversiteit Groningen, Nijenborgh 16, 9747 *AG Groningen, The Netherlands*

(*Received* 2 *February* 1979; *accepted* 12 *March* 1979)

Abstract

First-order TDS calculations have been made for naphthalene at 100 K to judge the suitability of different models for calculating TDS corrections used in practice. It appears that a long-wave model which takes account of the non-linearity of the frequency dispersion, gives about the same corrections for structural parameters as the lattice dynamical model for rigid body molecules and harmonic vibrations. Long-

0567-7394/79/040675-10$01.00

wave models with linear frequency dispersion give an overcorrection of the errors. For second-order TDS no explicit comparison of the models has been possible, but rough estimates show that the comparison made for first-order TDS is also valid in good approximation for the total TDS.

1. Introduction

As has been noticed by different authors, *e.g.* Willis (1969; see his Fig. 1), the contribution of thermal diffuse scattering (TDS) to integrated reflection intensities for X-ray and neutron diffraction, is not eliminated by the usual background correction. This is due to the fact that the TDS has a maximum below the Bragg peak. The TDS contribution to the intensity of a reflection **H** is given by

$$I(\mathrm{TDS},\mathbf{H}) = \int_{V_p(\mathbf{H})} I(\mathrm{TDS},\mathbf{S})\,\mathrm{d}\mathbf{S} - \frac{V_p(\mathbf{H})}{V_b(\mathbf{H})} \int_{V_b(\mathbf{H})} I(\mathrm{TDS},\mathbf{S})\,\mathrm{d}\mathbf{S}, \quad (1)$$

where $V_p(\mathbf{H})$ and $V_b(\mathbf{H})$ are the volumes in reciprocal space seen by the counter during the peak and background scan respectively (scanned volumes; Helmholdt & Vos, 1977), and **S** is a vector in reciprocal space. Several authors have calculated TDS corrections, $I(\mathrm{TDS},\mathbf{H})$, for reflection intensities. However, in general, for crystals with low symmetry, TDS corrections are determined from elastic constants and are thus based on a long-wave model with linear frequency dispersion for the acoustic modes (LW model). In the present paper, for a molecular crystal, naphthalene at 100 K, a lattice dynamical model is used to eliminate the TDS errors. To facilitate the computations the model assumes the molecules to be rigid and the thermal vibrations to be harmonic. A justification of the rigid-body assumption is that the lower lying phonon dispersion branches which mainly determine the TDS, are hardly affected by the non-rigidity of the molecules (Pawley & Cyvin, 1970). The lattice dynamical results will be compared with those of approximate methods. For this comparative study we have not used scanned volumes $V_p(\mathbf{H})$ and $V_b(\mathbf{H})$ as encountered in practice, but for all reflections the volumes V_p and V_b, respectively, have been taken as the same (§ 7.1).

2. The lattice dynamical model

The lattice dynamical formulae (Cochran, 1963; Hoppe, 1964; Willis, 1969; Pawley, 1972; Maradudin, Montroll & Weiss, 1963; Born & Huang, 1968) are briefly summarized below.

For τ rigid bodies m, $m = 1 - \tau$, in the primitive unit-cell, there are 6τ phonon dispersion branches σ. The dynamical behaviour of the crystal may be given by a sum of travelling waves for the translational and librational motions;

$$q_j(\sigma\mathbf{k};lmt) = q_j(\sigma\mathbf{k}m)\exp i[2\pi\mathbf{k}.\mathbf{r}(lm) - \omega(\sigma\mathbf{k})\,t], \quad (2)$$

$q_j(\sigma\mathbf{k}m)$, $j = 1$–3, stands for the translational components $t_j^s(\sigma\mathbf{k}m)$ or the librational components $\lambda_j^s(\sigma\mathbf{k}m)$ of mode $(\sigma\mathbf{k})$; $\mathbf{k}$ = wave vector, $\omega(\sigma\mathbf{k})$ = angular frequency, l = unit-cell index, $\mathbf{r}(lm)$ = position of gravity centre of m in cell l, t = time. For each wave vector $\mathbf{k}$ the angular frequencies $\omega(\sigma\mathbf{k})$ and the mass-adjusted amplitude vectors $\mathbf{t}^0(\sigma\mathbf{k}m)$ and $\boldsymbol{\lambda}^0(\sigma\mathbf{k}m)$ are obtained from the eigenvalues $\omega^2(\sigma\mathbf{k})$ and the eigenvectors $\mathbf{U}^0(\sigma\mathbf{k})$ of the $(6\tau \times 6\tau)$-dimensional dynamical matrix $D(\mathbf{k})$. For the mass adjustment of $t_j^0(\sigma\mathbf{k}m)$, the mass $M_{jj}(m) = M(m)$ is used, and for that of $\lambda_j^0(\sigma\mathbf{k}m)$ the inertial moment $I_{jj}(m)$. The non-mass-adjusted components are given by

$$t_j(\sigma\mathbf{k}m) = M_{jj}^{-1/2}(m)\,t_j^0(\sigma\mathbf{k}m), \quad (3a)$$

$$\lambda_j(\sigma\mathbf{k}m) = I_{jj}^{-1/2}(m)\,\lambda_j^0(\sigma\mathbf{k}m). \quad (3b)$$

In general the components $t_j(\sigma\mathbf{k}m)$ and $\lambda_j(\sigma\mathbf{k}m)$ are complex. For naphthalene where the molecules lie at inversion centres, the translational and librational components have a phase difference of $\pi/2$ (Pawley, 1967) and for each of the modes the translational components can be assumed to be purely real, and the librational components to be purely imaginary. The different modes are dynamically independent (James, 1965, p. 198).

The scaled amplitudes $\mathbf{t}^s$ and $\boldsymbol{\lambda}^s$ are obtained from $\mathbf{t}$ and $\boldsymbol{\lambda}$ by multiplication with the scale factor

$$C(\sigma\mathbf{k}) = [E(\sigma\mathbf{k})/N\omega^2(\sigma\mathbf{k})]^{1/2}, \quad (4)$$

where $E(\sigma\mathbf{k})$ is the energy of the mode $\sigma\mathbf{k}$ and N the number of primitive cells considered. As quantum effects can be neglected for the present calculations (Helmholdt & Vos, 1977), the expression for the energy is

$$E(\sigma\mathbf{k}) = k_B\,T, \quad (5)$$

with k_B the Boltzmann constant and T the absolute temperature.

TDS intensity

The first-order TDS intensity $I_1(\mathrm{TDS};\ \mathbf{S} = \mathbf{H} - \mathbf{k})$ per unit reciprocal volume at $\mathbf{S} = \mathbf{H} - \mathbf{k}$ is given by

$$I_1(\mathrm{TDS};\ \mathbf{S} = \mathbf{H} - \mathbf{k}) = 4\pi^2 S^2 N \sum_\sigma \frac{k_B\,T}{\omega^2(\sigma\mathbf{k})} |F_1(\mathbf{S}\sigma\mathbf{k})|^2, \quad (6)$$

with $S = 2\sin\theta/\lambda$; $|F_1(\mathbf{S}\sigma\mathbf{k})|$ is the structure factor amplitude for first-order TDS and reads

$$|F_1(\mathbf{S}\sigma\mathbf{k})| = \left|\sum_{ma} f(\mathbf{S}ma)\,\hat{\mathbf{s}}.\mathbf{p}(\sigma\mathbf{k};ma) \times \exp 2\pi i[\mathbf{H}.\mathbf{r}(m) + \mathbf{S}.\mathbf{r}(ma)]\right|, \quad (7)$$

ma = index for atoms a of rigid body m, $f(\mathbf{S},ma)$ = scattering factor of atom ma, including the temperature factor, $\mathbf{r}(m)$ = position vector of gravity centre of m, $\mathbf{r}(ma)$ = position vector of atom ma relative to $\mathbf{r}(m)$; $\mathbf{r}(m) + \mathbf{r}(ma)$ gives the position of atom ma in the unit cell; $\hat{\mathbf{s}}$ = unit vector in direction $\mathbf{S}$; $\mathbf{p}(ma)$ is the (non-scaled) displacement vector of atom ma. For the rigid body model this displacement reads

$$\mathbf{p}(\sigma\mathbf{k};ma) = \mathbf{t}(\sigma\mathbf{k}m) + \boldsymbol{\lambda}(\sigma\mathbf{k}m) \times \mathbf{r}(ma). \quad (8)$$

The second-order TDS intensity per unit reciprocal volume at $\mathbf{S} = \mathbf{H} - \mathbf{k}$ with $\mathbf{k} = \mathbf{k}' + \mathbf{k}''$ is called $I_2(\text{TDS}; \mathbf{S} = \mathbf{H} - \mathbf{k})$ and is given by

$$I_2(\text{TDS}; \mathbf{S} = \mathbf{H} - \mathbf{k}) = 8\pi^4 NS^4 \int_{\mathbf{k}'} \sum_{\sigma'} \sum_{\sigma''} \frac{(k_B T)^2}{\omega^2(\sigma'\,\mathbf{k}')\,\omega^2(\sigma''\,\mathbf{k}'')} \times |F_2(\mathbf{S}\sigma'\,\mathbf{k}'\,\sigma''\,\mathbf{k}'')|^2 \frac{\mathrm{d}\mathbf{k}'}{v^*}, \quad (9)$$

with integration over the whole Brillouin zone (BZ); $v^* = [V(\text{cell})]^{-1}$ and

$$F_2(\mathbf{S}\sigma'\,\mathbf{k}'\,\sigma''\,\mathbf{k}'') = \sum_{ma} f(\mathbf{S}ma)\,\hat{\mathbf{s}}.\mathbf{p}(\sigma'\,k';ma) \times \hat{\mathbf{s}}.\mathbf{p}(\sigma''\,\mathbf{k}'';ma) \times \exp 2\pi i[\mathbf{H}.\mathbf{r}(m) + \mathbf{S}.\mathbf{r}(ma)]. \quad (10)$$

The intensities $I_1(\text{TDS},\mathbf{H})$ and $I_2(\text{TDS},\mathbf{H})$ obtained by integration of (6) and (9), respectively, over reciprocal space according to (1), can be compared with the Bragg intensity

$$I(\text{Bragg},\mathbf{H}) = Nv^*|F_B(\mathbf{H})|^2, \quad (11)$$

where $F_B(\mathbf{H})$ is the usual structure factor

$$F_B(\mathbf{H}) = \sum_{ma} f(\mathbf{S}ma) \exp 2\pi i\mathbf{H}.[\mathbf{r}(m) + \mathbf{r}(ma)]. \quad (12)$$

3. Long-wave models

Among the 6τ branches there are three acoustic branches σ_a, σ_a = 1–3, which for $\mathbf{k} \to 0$, and thus for long waves, obey the relations

$$\omega(\sigma\mathbf{k}) = 2\pi v(\sigma\hat{\mathbf{k}})\,k, \quad (13a)$$

$$\boldsymbol{\lambda}^{\text{LW}}(\sigma_a\,\mathbf{k}m) = 0, \quad (13b)$$

$$\mathbf{t}^{\text{LW}}(\sigma_a\,\hat{\mathbf{k}}m) = \mathbf{t}(\sigma_a\,\hat{\mathbf{k}}), \quad (13c)$$

with $\hat{\mathbf{k}} = \mathbf{k}/k$, $v(\sigma\hat{\mathbf{k}})$ = sound velocity for direction $\hat{\mathbf{k}}$. The long-wave translational amplitude vectors are real and equal for the different molecules m, the frequency dispersion is linear and velocities and $\mathbf{t}^{\text{LW}}$ vectors depend only on the direction and not on the magnitude of $\mathbf{k}$. All rigid bodies adjust themselves by translational motion only to the waves (in non-scaled formulation)

$$\mathbf{t}^{\text{LW}}(\sigma_a\,\mathbf{k};lmt) = \mathbf{t}^{\text{LW}}(\sigma_a\,\mathbf{k}) \exp i[2\pi\mathbf{k}.\mathbf{r}(lm) - \omega(\sigma\mathbf{k})\,t]. \quad (14)$$

From (13a), (6) and (9) we see that the TDS peak for $\mathbf{S} \to \mathbf{H}$ or for $\mathbf{k} \to 0$ is caused predominantly by the acoustic modes with low frequency. Therefore, often long-wave TDS models are applied which are based on the assumption that the acoustic long-wave character for $\mathbf{k} \to 0$ also holds for larger values of $\mathbf{k}$. We have used two types of models.

I. The long-wave model with following rigid bodies (LWF model). The above situation with formulae (13a), (13c) and (14) holds. The first-order TDS is given by

$$I_1^{\text{LWF}}(\text{TDS}, \mathbf{S} = \mathbf{H} - \mathbf{k}) = 4\pi^2 NS^2 k_B T \Big|\sum_{ma} f(\mathbf{S}ma) \exp 2\pi i[\mathbf{H}.\mathbf{r}(m) + \mathbf{S}.\mathbf{r}(ma)]\Big|^2 \sum_{\sigma_a} \{[\hat{\mathbf{s}}.\mathbf{t}^{\text{LW}}(\sigma_a\,\hat{\mathbf{k}})]/2\pi v(\sigma_a\,\hat{\mathbf{k}})\,k\}^2. \quad (15)$$

II. The long-wave model with following atoms (LWA model). In this case each individual atom is considered as a rigid body which adjusts itself by translational motion to the acoustic waves. In the TDS formulae $[\mathbf{H}.\mathbf{r}(m) + \mathbf{S}.\mathbf{r}(ma)]$ is replaced by $[\mathbf{H}.\mathbf{r}(m) + \mathbf{H}.\mathbf{r}(ma)]$ so that we obtain from (15), (13a), (6), (7), (9), (10) and (12)

$$I_1^{\text{LWA}}(\text{TDS}, \mathbf{S} = \mathbf{H} - \mathbf{k}) = 4\pi^2 NS^2 k_B T |F_B(\mathbf{H})|^2 \sum_{\sigma_a} \{[\hat{\mathbf{s}}.\mathbf{t}^{\text{LW}}(\sigma_a\,\mathbf{k})]/\omega(\sigma_a\,\mathbf{k})\}^2 \quad (16)$$

and

$$I_2^{\text{LWA}}(\text{TDS}, \mathbf{S} = \mathbf{H} - \mathbf{k}) = 8\pi^4 NS^4 |F_B(\mathbf{H})|^2 \times \int_{\mathbf{k}'} \sum_{\sigma_a'} \sum_{\sigma_a''} \frac{(k_B T)^2}{\omega^2(\sigma_a'\,\mathbf{k}')\,\omega^2(\sigma_a''\,\mathbf{k}'')} \times [\hat{\mathbf{s}}.\mathbf{t}^{\text{LW}}(\sigma_a'\,\mathbf{k}')\,\hat{\mathbf{s}}.\mathbf{t}^{\text{LW}}(\sigma_a''\,\mathbf{k}'')]^2 \frac{\mathrm{d}\mathbf{k}'}{v^*}. \quad (17)$$

For this model two cases have been distinguished:

II. (*A*) Linear frequency dispersion according to (13*a*). The resulting model is called the LW model. The TDS expressions are given by (16) and (17) with (13*a*) for the frequencies.

II. (*B*) Non-linear frequency dispersion. This model is called the LWD model. In the TDS expressions (16) and (17) correct values for $\omega(\sigma_a \mathbf{k})$ are used, which can be derived either from experimental data or, as has been done in the present paper, from lattice dynamical calculations.

Model II(*A*) has been considered as it is often applied in crystallographic studies (Willis, 1969; Cochran, 1969), and model I has been compared with II(*A*) to check the difference caused by the adjustment of rigid bodies rather than individual atoms to the waves.

4. Choice of potential functions

The force constants required for the dynamical matrix $D(\mathbf{k})$ have been calculated with the following assumptions: (*a*) the force on molecule *m* is the sum of the forces on its atoms *ma*; (*b*) the forces on the atoms are obtained from pair-potential functions of the Buckingham type,

$$V(r_{ij}) = -Ar_{ij}^{-6} + B\exp(-Cr_{ij}), \qquad (18)$$

where $V(r_{ij})$ gives the interaction energy between two atoms *i* and *j* at distance r_{ij}. The constants *A*, *B* and *C* depend on the types of atoms considered. As the peaking of the TDS below the Bragg peak is directly connected with the wave velocity, published sets of *A*, *B* and *C* values for C···C, H···H and C···H interactions (Williams, 1966, 1967, 1970, 1974; Taddei, Bonadeo, Marzocchi & Califano, 1973; Mirskaya, Kozlova & Bereznitskaya, 1974) were tested on their ability to reproduce the velocities of elastic waves measured for different crystals (Kroon, 1977). In addition to variations in *A*, *B* and *C*, variations in C–H distances were considered. For different parameter sets, best agreement with measured sound velocities was obtained for C–H = 1·09 Å. Differences between observed and calculated elastic wave velocities for different sets of *A*, *B* and *C* values and C–H = 1·09 Å are given in Table 1. On the basis of this table, set (*d*) was chosen for the further TDS calculations, although sets (*a*)–(*c*) and set (*e*) seem to be nearly as good.

5. Thermal motion

The naphthalene molecules lie at inversion centres in the cell. Starting from the structure determined by Cruickshank (1957), rotations of 1·6, 0·3 and 1·3° respectively about the axes of inertia were applied to minimize the energy in the assumed potential field. The cell dimensions were kept constant. The minimization procedure is essentially the same as that described by Filippini, Gramaccioli, Simonetta & Suffritti (1973), apart from the fact that we have taken a summation limit of 7 Å instead of 5·5 Å. The resulting coordinates are listed in Table 2. For carbon $\sum_i (\Delta q_i)^2 = 0{\cdot}02$ (function of merit, defined by Filippini *et al.*), where Δq_i is the change in coordinate q_i, in Å, relative to the Cruickshank structure. For the coordinates and cell parameters of Table 2 the **T** and **L** tensors at 300 K were calculated with the formulae (Scheringer, 1973*b*)

$$T_{ij}(m) = k_B T \,\mathrm{Re}\left[\sum_{\sigma\mathbf{k}} t_i(\sigma\mathbf{k}m)\, t_j(\sigma\mathbf{k}m)/\omega^2(\sigma\mathbf{k})\right], \quad i, j = 1\text{–}3, \qquad (19a)$$

$$L_{ij}(m) = k_B T \,\mathrm{Re}\left[\sum_{\sigma\mathbf{k}} \lambda_i(\sigma\mathbf{k}m)\, \lambda_j(\sigma\mathbf{k}m)/\omega^2(\sigma\mathbf{k})\right]. \qquad (19b)$$

The tensor $\mathbf{S} = 0$ as the molecule lies at an inversion centre. The procedure for the summation over the BZ has been described by Kroon & Vos (1978); an evenly spaced grid with intervals of $(1/24)\,\mathbf{a}^*$, $(1/24)\,\mathbf{b}^*$ and $(1/24)\,\mathbf{c}^*$ was applied.

Comparison of the present **T** and **L** tensors with Pawley's (1967) values shows that

$$\frac{\langle T_{ii}(\text{present})\rangle}{\langle T_{ii}(\text{Pawley})\rangle} = 1{\cdot}313, \quad \frac{\langle L_{ii}(\text{present})\rangle}{\langle L_{ii}(\text{Pawley})\rangle} = 1{\cdot}313.$$

We have ascribed the relatively low values obtained by Pawley to the use of an insufficiently dense summation grid (Gramaccioli, Simonetta & Suffritti, 1973), although it is surprising that for the libration the percentage discrepancy is as large as for the translation. In Table 3 the present values are compared with those of Pawley (after multiplication by 1·313) and with the **T** and **L** tensors calculated by Filippini, Gramaccioli, Simonetta & Suffritti (1973). The three sets show an analogous trend. Closer inspection shows, however, that the T_{ii} values of Filippini *et al.* (1973), especially that for T_{11}, tend to be higher than the present values, while their values for L_{ii} tend to be somewhat lower. There are two possible explanations for the observed differences. (1) The difference in parameter set. Set (*e*) of Table 1, which is the Williams IV*a* set used by Filippini *et al.*, gives lower wave velocities (Kroon, 1977), and thus higher T_{ii} values, than set (*d*). (2) The summation technique. From Table 3 in Gramaccioli, Simonetta & Suffritti (1973), we see that non-convergence in their summation technique makes T_{ii} too high and L_{ii} too low. For the present summation, on the other hand, we expect an underestimate of 3·5% for T_{11} and of about 1% for T_{22} and T_{33}, whereas convergence has been reached for L_{ii} (Kroon & Vos, 1978).

Table 1. *Tested parameter sets A, B and C for potential functions* (18), *and differences between observed and calculated values for lattice frequencies and elastic wave velocities*

Given are (left) r.m.s. differences defined as $\{\sum[p(\text{calc}) - p(\text{exp})]^2/n\}^{1/2}$, and (right) average differences defined as $\{\sum[p(\text{calc}) - p(\text{exp})]\}/n$, n = number of parameters p; C–H = 1·09 Å.

	C···C			H···H			C···H		
Set*	*A*	*B*	*C*	*A*	*B*	*C*	*A*	*B*	*C*
(*a*)	602	89290	3·60	71	4000	3·74	86	6767	3·67
(*b*)	440	43380	3·60	58	4000	3·74	160	13170	3·67
(*c*)	437	44010	3·60	50	4000	3·74	168	13270	3·67
(*d*)	535	74460	3·60	36	4000	3·74	139	9411	3·67
(*e*)	568	83630	3·60	27·3	2654	3·74	125	8766	3·67
(*f*)	538·7	74620	3·60	17·93	1704	3·74	96·8	7703	3·67
(*g*)	512·6	71782	3·60	24·4	2171	3·74	111·8	8503	3·67
(*h*)	449·3	71462	3·60	40·1	2868	3·74	134·2	5667	3·67
(*i*)	421	71600	3·68	29	4900	4·29	118	18600	3·94
(*j*)	566·7	78659	3·61	26·5	2260	3·74	127·6	8810	3·67

	Lattice frequencies (cm^{-1})						Elastic velocities (10 m/s)					
Set	NF†		AN		BZ138		NF		AN		BZ218	
(*a*)	10	−7	2	−1	14	−12	37	−23	30	−18	34	−24
(*b*)	11	2	14	10	7	−2	37	−12	26	−8	42	−4
(*c*)	11	3	14	11	7	−1	39	−12	27	−6	40	−2
(*d*)	9	0	7	6	7	−3	35	−18	25	−9	29	−9
(*e*)	10	−7	3	−1	13	−11	33	−21	25	−19	32	−18
(*f*)	14	−13	8	−6	20	−19	45	−37	38	−34	42	−32
(*g*)	12	−10	5	−4	17	−15	40	−31	33	−30	38	−26
(*h*)	24	−22	20	−18	24	−24	72	−62	69	−62	63	−58
(*i*)	18	−17	11	−10	24	−23	56	−47	48	−44	47	−36
(*j*)	12	−10	8	−6	17	−15	43	−33	36	−30	49	−43

* The parameter sets used are (*a*)–(*d*) Williams (1966) set I–IV; (*e*) Williams (1967) set IV; (*f*)–(*g*) Williams (1970) set *A* and *C*; (*h*) Williams (1974); (*i*) Mirskaya *et al.* (1974); (*j*) Taddei *et al.* (1973).

† NF = naphthalene, AN = anthracene, BZ138 = benzene at 138 K. Experimental data for frequencies are from Harada & Shimanouchi (1966, 1967); Ito, Suzuki & Yokoyama (1968), Chantry, Gebbie, Lassier & Wyllie (1967), Bonadeo, Marzocchi, Castellucchi & Califano (1972). Experimental data for velocities are from Aleksandrov, Belikova, Rhyzenkov, Teslenko & Kitaigorodskii (1963), Afanas'eva, Aleksandrov & Kitaigorodskii (1967), Afanas'eva (1968), Teslenko (1967), Huntington, Gangoli & Mills (1969), Afanas'eva & Myasnikova (1970), Heseltine, Elliot & Wilson (1964).

Table 2. *Crystallographic data of naphthalene as used for the lattice dynamical calculations*

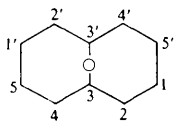

	x	*y*	*z*	U_{11}	U_{22}	U_{33}	U_{12}	U_{13}	U_{23}
C(1)	0·08319	0·02629	0·32404	3·052	3·061	1·907	0·241	1·330	−0·038
C(2)	0·10896	0·16574	0·21626	2·486	2·278	1·984	−0·080	1·048	−0·373
C(3)	0·04404	0·10449	0·03290	1·741	1·716	1·850	0·075	0·905	−0·039
C(4)	0·06823	0·24816	−0·08336	2·355	1·963	2·500	0·004	1·377	0·220
C(5)	0·00768	0·18329	−0·25743	2·926	2·765	2·418	0·332	1·659	0·549
H(1)	0·13292	0·07717	0·46397	4·578	4·468	2·057	0·253	1·759	−0·279
H(2)	0·17812	0·32576	0·26810	3·546	2·654	2·680	−0·596	1·361	−0·937
H(4)	0·13744	0·40978	−0·03165	3·325	2·095	3·609	−0·451	1·953	0·115
H(5)	0·02781	0·29566	−0·34449	4·250	3·720	3·313	0·450	2·558	1·168

Cell parameters
a = 8·235 Å
b = 6·003
c = 8·658
β = 122·55°*

Space group $P2_1/a$
coordinates listed are those after energy minimization by *LATDYN*

U_{ij}'s are calculated from **T** and **L** tensors obtained from lattice dynamical data and given in 10^{-2} Å^2

* For the present work by accident β = 122·55° has been taken instead of β = 122° 55′ = 122·91°.

Table 3. *Comparison of* **T** *and* **L** *tensors obtained by lattice dynamical calculations at* 300 K *(see text)*

The tensors are given in the inertial frame defined by Cruickshank (1957). T_{ij} in 10^{-4} Å^2 and L_{ij} in 10^{-1} degree^2.

	T_{11}	T_{22}	T_{33}	T_{12}	T_{13}	T_{23}
Present work	551	527	461	20	−15	−20
Pawley (1967) (×1·313)	544	544	452	11	−7	−24
Filippini *et al.* (1973)	600	532	478	13	−14	−28
	L_{11}	L_{22}	L_{33}	L_{12}	L_{13}	L_{23}
Present work	296	188	235	38	5	21
Pawley (1967) (×1·313)	287	206	226	34	8	32
Filippini *et al.* (1973)	271	182	232	29	6	17

6. Phonon dispersion curves and eigenvector dispersion

For the calculation of the frequencies and eigenvectors the Fortran program *LATDYN* has been written (Kroon, 1977). Fig. 1 shows the phonon dispersion curves for the **b*** direction. Especially for higher **k** values, the acoustic branches do not obey (13*a*), as expected.

To get an impression to what extent the acoustic character of the eigenvectors of the acoustic modes

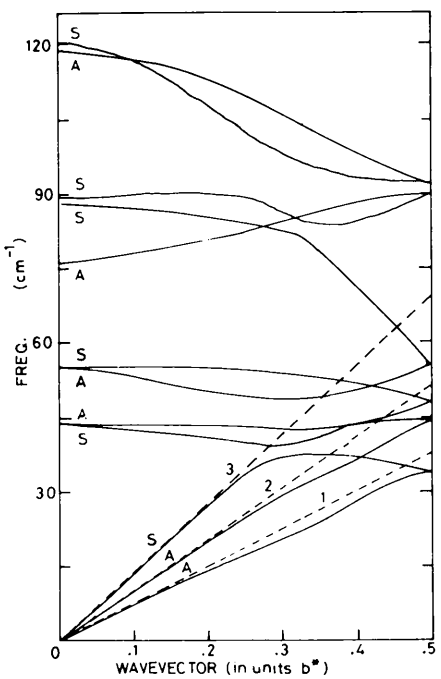

Fig. 1. Dispersion curves for the $|0k0|$ direction in naphthalene calculated with the lattice dynamical rigid-body model. The dashed line illustrates the frequencies in case of linear dispersion. *S* and *A* indicate symmetric and antisymmetric modes respectively.

(σ_a **k**) at **k** → 0 is retained at higher **k** values, we have calculated the so-called eigenvector dispersion

$$\mathrm{ED}(\sigma_a \mathbf{k}) = \sum_{\sigma} |\mathbf{U}^{0T}(\sigma_a, \mathbf{k}\ \text{small})\, \mathbf{U}^{*0}(\sigma \mathbf{k})|^2 \times \omega^2(\sigma_a \mathbf{k})/\omega^2(\sigma \mathbf{k}). \quad (20)$$

For **k** small, values of typically 10^{-4} Å^{-1} were taken; $k = 0$ cannot be used as a reference since the acoustic modes are degenerate at this point. The factor $\omega^2(\sigma_a k)/\omega^2(\sigma k)$ accounts for the difference in scaling (4) between the modes. Fig. 2 shows for **k** along **b*** for each of the branches σ_a the values ED(σ_a **k**;tot) where tot stands for the total number of branches considered in the summation (20). For tot = 1 the summation is over $\sigma = \sigma_a$ only, for tot = 3 over all three acoustic branches and for tot = 12 over all twelve branches. Also the average quantity

$$\langle \mathrm{ED}(\mathbf{k};12) \rangle = \left[\sum_{\sigma_a} \omega^{-2}(\sigma_a \mathbf{k}) \times \mathrm{ED}(\sigma_a \mathbf{k};12) \right] \Big/ \left[\sum_{\sigma_a} \omega^{-2}(\sigma_a \mathbf{k}) \right] \quad (21)$$

is given, in which according to the scaling (4) the contribution of each mode (σ_a **k**) has been weighted with $\omega^{-2}(\sigma_a \mathbf{k})$. We see that for **k** = 0·2**b***, the acoustic character is retained for 95% on average and for **k** = 0·5**b*** for 66%. Fig. 2 shows that at **k** = 0·31**b*** the character of the symmetric acoustic branch three is taken over by the lowest lying symmetric optic branch four, whereas the eigenvectors $\mathbf{U}^0(3;\mathbf{k}\ \text{small})$ and $\mathbf{U}^0(3;\mathbf{k} > 0{\cdot}31\mathbf{b}^*)$ are almost orthogonal. Note further that for branch three ED(3**k**;3) = ED(3**k**;1) as the symmetric and antisymmetric acoustic modes do not combine with each other.

7. First-order TDS calculations

7.1. *Setup of the calculations*

TDS intensities were calculated with the Fortran program *TDS* (Kroon, 1977). Again a division of each

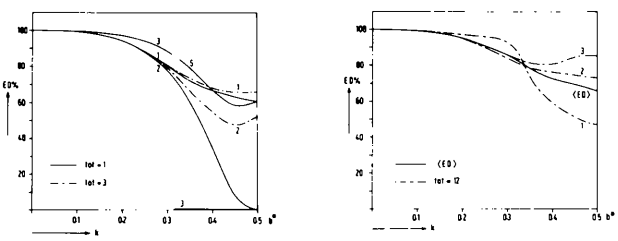

Fig. 2. Eigenvector dispersion ED(×10^2) along **b*** for the three acoustic branches. Curves are given for different tot values (see text) and for ⟨ED⟩ defined by (21). Curve *S* gives $|\mathbf{U}^{0T}(3;\mathbf{k}\ \text{small})\, \mathbf{U}^{0*}(4\mathbf{k})|^2$. For **k** < 0·25**b*** the tot = 3 curves approach the corresponding tot = 1 curves very closely.

reciprocal axis into 24 intervals was used. Frequencies and eigenvectors were obtained with the program *LATDYN* for 7488 **k** values in half the BZ [the other half is found by the simple relations $\omega^2(\sigma\mathbf{k}) = \omega^2(\sigma,-\mathbf{k})$ and $\mathbf{U}^0(\sigma\mathbf{k}m) = \mathbf{U}^{0*}(\sigma,-\mathbf{k}m)$].

To simulate the TDS errors for data measured at 100 K, we have taken the Cruickshank (1957) structure after energy minimization with **T** and **L** tensors as expected for 100 K. These tensors were obtained by dividing the **T** and **L** values of Table 3 by three. The corresponding **U** tensors and the coordinates after energy minimization are given in Table 2. For this structure in the range up to $\sin\theta/\lambda = 1{\cdot}2$ Å^{-1} one of each five reflections was taken leaving 1077 independent reflections. The volume V_p was taken congruent with the reciprocal unit-cell shape. It is centred around **H** and has edges of 0·292 (0·146 on either side) **a***, **b*** and **c***. The background TDS intensity was calculated by extending the scanned volume V_p by one grid interval (on either side) in the **a*** direction. The largest wave vectors considered at $\sin\theta/\lambda = 1{\cdot}0$ Å^{-1} are 0·045 Å^{-1} (0·27**b***) for the present calculations and 0·038 Å^{-1} for the practical conditions chosen by Helmholdt & Vos (1977). The present volume is thus sufficiently large to obtain a good estimate of TDS effects occurring in practical cases.

7.2. *Influence of the optic modes. The EX model*

On the basis of the lattice dynamical model, for a restricted number of reflections, I_1(TDS,**H**) values were computed both with inclusion of all modes, $\sigma = 1$–12, and with the acoustic modes, σ_a, only. Data for some reflections are listed in Table 4. For none of the reflections is the contribution of the optical modes >1·5% of the acoustical contribution. This shows that for the present case the neglect of optical modes, usually applied in the calculation of first-order TDS corrections, is justified. Therefore in all further calculations of first-order TDS intensities acoustic modes only have been considered. The result of the lattice dynamical calculations based on the acoustic modes are indicated as EX(act).

7.3. *First-order TDS profiles and* α_1(**H**) *values for different models*

Fig. 3 shows the first-order TDS profiles along **b*** for the LW, LWF, LWD and EX models. The numbers indicate the positions of the reflections 0*k*0. In agreement with the fact that the LW and LWD thermal diffuse scattering is proportional to $|F_B(\mathbf{H})|^2$ (16), the LW and LWD TDS intensities are zero around the systematically absent reflections 0*k*0 with *k* odd. For these reflections zero TDS intensity is also expected along **b*** for LWF as can be seen by substitution of $\Delta y = \frac{1}{2}$ for the positions of the molecular centres in (15). For the EX model the TDS intensity is not zero around the systematically absent reflections, but the profile is so smooth that TDS errors are expected to be eliminated by the usual background corrections. At the positions of the reflections 0*k*0 with *k* even, for all models the TDS intensity goes to infinity. In practice no infinite intensity will be measured due to finite resolution of the experimental setup (Cochran, 1969; Jennings, 1970; Walker & Chipman, 1970; Scheringer, 1973*a*; Stevens, 1974).

Table 5 shows the values

$$\alpha_1(\mathbf{H}) = I_1(\text{TDS},\mathbf{H})/I(\text{Bragg},\mathbf{H}) \qquad (22)$$

for the four models and a set of randomly chosen reflections. We see that the $\alpha_1^{EX}(\mathbf{H})$ values show a strong anisotropy and that for some high-order reflections values higher than 100% are reached. Both the LW and LWF models overestimate the TDS errors and in most cases $\alpha_1^{LWF}(\mathbf{H})$ deviates more from $\alpha_1^{EX}(\mathbf{H})$ than $\alpha_1^{LW}(\mathbf{H})$. Values which lie considerably closer to $\alpha_1^{EX}(\mathbf{H})$ are obtained with the LWD model. This makes it clear

Table 4. *Comparison of* $|F_B|^2$ *and the net first-order TDS intensity due to acoustic and optic branches for some reflections distributed through reciprocal space*

h	*k*	*l*	sin θ/λ	$\lvert F_B\rvert^2$	I_1(ac)	I_1(opt)
1	1	−2	0·142	141·1	0·8587	0·002
0	2	0	0·167	258·0	2·811	0·005
1	1	3	0·265	138·0	3·741	0·001
4	0	−5	0·307	26·18	1·111	0·006
5	5	−6	0·559	75·41	9·645	0·011
9	3	−4	0·606	41·33	8·470	0·010
0	7	5	0·676	13·43	2·258	0·003
2	5	−12	0·868	5·958	1·089	0·001
4	10	−8	0·953	0·5538	0·2025	0·002
2	8	9	0·970	1·509	0·6116	0·002
5	4	11	1·049	0·1454	0·0770	0·001
10	3	−18	1·071	0·6573	0·3363	0·002
17	1	−1	1·192	0·0112	0·0150	0·000

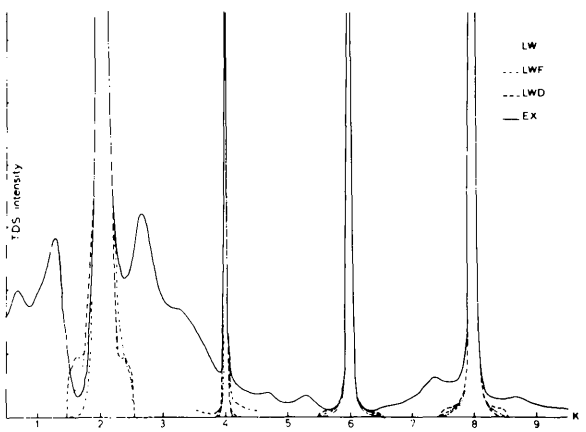

Fig. 3. First-order TDS intensity profiles along **b*** in naphthalene, calculated with LW, LWF, LWD and EX methods. The numbers give the positions of the 0*k*0 reflections.

Table 5. *Comparison of $\alpha_1(\mathbf{H})$ values calculated by the EX and by different approximate TDS methods for an arbitrarily chosen set of reflections*

$\alpha_1(\mathbf{H})$ is defined by (22) and given in %.

h	k	l	$\sin\theta/\lambda$	$10^3\lvert F_B\rvert^2$	α_1^{LW}	α_1^{LWF}	α_1^{LWD}	α_1^{EX}
0	1	3	0·2217	55606	1·4	1·5	1·3	1·3
4	5	−1	0·4898	6123	14·9	15·1	12·5	12·5
2	5	3	0·5178	406	12·6	13·2	11·1	10·7
1	6	−4	0·5557	1000	10·9	11·0	10·8	10·3
6	0	−10	0·5810	7167	11·2	11·6	9·8	10·0
6	6	−5	0·6282	40192	22·8	22·9	19·4	19·3
12	1	−6	0·7353	5096	62·5	64·7	45·4	44·4
9	5	−9	0·7375	4957	34·1	34·5	27·6	27·4
7	1	5	0·7507	673	45·9	52·1	33·7	32·5
8	2	4	0·7772	138	53·3	64·1	39·0	37·1
7	8	−10	0·8922	10·5	32·5	157·8	29·7	22·9
10	0	4	0·8973	110	76·6	67·1	55·5	62·7
8	9	0	0·9453	2252	59·9	59·4	49·0	49·0
0	5	13	0·9829	1288	28·7	28·5	25·7	25·9
3	6	−14	0·9964	110	24·3	23·6	23·8	23·8
11	4	4	1·0228	186	94·9	95·8	69·8	69·0
17	1	−11	1·0399	116	115·1	118·8	84·5	81·1
12	9	−3	1·0769	62·9	94·5	94·9	73·9	76·0
0	13	1	1·0850	32·2	46·1	43·6	45·5	46·6
2	13	−5	1·1214	0·651	47·7	89·1	47·1	34·7
15	7	−14	1·1457	36·2	91·2	92·5	72·7	52·1
10	7	6	1·1597	34·3	100·1	103·2	76·5	73·2
1	14	−1	1·1680	91·1	53·6	53·3	52·9	53·6
3	13	5	1·1899	45·4	60·2	60·1	56·2	57·0
13	8	−16	1·1909	75·7	70·7	71·4	59·7	60·0
4	13	−9	1·2018	18·7	52·1	54·6	51·2	51·3
18	6	−8	1·2109	40·9	154·4	155·2	114·4	113·2

that for naphthalene-type crystals a long-wave model with flexible molecules and correct $\omega(\sigma\mathbf{k})$ dispersion gives good estimates for the first-order TDS errors, and that neglect of eigenvector dispersion as shown in Fig. 2 by ED($\sigma_a\mathbf{k}$;3) does not have a large effect on $\alpha_1(\mathbf{H})$. The noticeable influence of the non-linearity of the frequency dispersion arises from the fact that the scanned volume V_p extends to 0·3, and the background region to about 0·4 the BZ boundary. For practical intensity measurements sometimes even larger $\mathbf{k}$ values are encountered in scanned reciprocal volumes (Helmholdt, 1975).

8. Higher-order TDS

The total TDS error $I(\text{TDS},\mathbf{H})$ of (1) contains in addition to the first-order TDS error $I_1(\text{TDS},\mathbf{H})$, the contributions $I_2(\text{TDS},\mathbf{H})$ *etc.* of higher-order TDS. From the TDS data given for NaF by Cochran (1969), it can be deduced that $I(\text{TDS},\mathbf{H})$ is mainly due to first-order scattering, and that the contributions of third and higher order scattering can be neglected. For molecular crystals it has been found (Stevens, 1974) that $I_2(\text{TDS},\mathbf{H}) \simeq 0{\cdot}2I_1(\text{TDS},\mathbf{H})$ for high-order reflections ($\sin\theta/\lambda \simeq 1{\cdot}0$ Å^{-1}). For lower-order reflections, second-order TDS is even less important, because of the proportionality of first- and second-order TDS to S^2 and S^4 respectively.

In the program *TDS* (Kroon, 1977) the option of calculating intensity distributions $I_2(\text{TDS};\mathbf{S}=\mathbf{H}-\mathbf{k})$ and errors $I_2(\text{TDS},\mathbf{H})$ for second-order TDS, has been incorporated, both for the lattice dynamical and the long-wave models. A numerical comparison of the different models has not been possible, however, because of the excessively high computing time required for the lattice dynamical calculations. For just one point in reciprocal space, the computation of $I_2(\text{TDS};\mathbf{S}=\mathbf{H}-\mathbf{k})$ took 800 cpu s on a Cyber 74-16, even when only three branches were considered in the summation given by (9). However, as $I_2(\text{TDS},\mathbf{H})$ is one order of magnitude smaller than $I_1(\text{TDS},\mathbf{H})$, errors of some 10–20% in $I_2(\text{TDS},\mathbf{H})$ will not affect the total error more than the differences found between the LWD and EX model for first order TDS (Table 5). We do not think it likely that this 10–20% will be exceeded by use of the LWD model for $I_2(\text{TDS},\mathbf{H})$ on the basis of the following three arguments. (1) The larger part of $I_2(\text{TDS},\mathbf{H})$ is due to (acoustic) modes with small $\mathbf{k}$; for a spherically scanned volume with radius r, the contribution of modes with $k < r$ has been estimated to be about 80% (Reid, 1973). (2) The optic branches of naphthalene are reasonably flat (Fig. 1) and at $\mathbf{k}=0{\cdot}5\mathbf{b}^*$ still 66% of the acoustic character is retained (§ 6). (3) For $I_2(\text{TDS},\mathbf{H})$ the percentage error due to neglect of the librational character of the acoustic modes will be smaller than for $\lvert F_2(\mathbf{S}\sigma'\,\mathbf{k}'\,\sigma''\,\mathbf{k}'')\rvert^2$, as for the different combinations $(\sigma'\,\mathbf{k}')$, $(\sigma''\,\mathbf{k}'')$ used during the integrations (9) and (1) the errors in the $\lvert F_2(\mathbf{S}\sigma'\,\mathbf{k}'\,\sigma''\,\mathbf{k}'')\rvert^2$ intensities may be different in magnitude and in sign, see (8) and (10).

In addition to the above remarks on the LWD model, it is easy to show that second- and first-order TDS are analogous with respect to the fact that neglect of non-linearity of the frequency dispersion makes the calculated $I(\text{TDS},\mathbf{H})$ error too high. It is therefore reasonable to assume that the conclusions obtained in the next paragraph from the comparison of the different models for first-order TDS are also valid for the total TDS in good approximation.

9. Influence of first-order TDS errors on structural parameters

Least-squares refinements

The influence of TDS errors on the structural parameters was determined by least-squares refinement on structure amplitudes $\lvert F_o(\mathbf{H})\rvert$ calculated from the relation

$$\lvert F_o(\mathbf{H})\rvert^2 = \lvert F_B(\text{model};\mathbf{H})\rvert^2[1+\alpha_1(\mathbf{H})]. \quad (23)$$

$F_B(\text{model};\mathbf{H})$ is based on the naphthalene model of Table 2. $\alpha_1(\mathbf{H})$ values for the EX, LW, LWF and LWD models are considered. The function minimized is

$$Q(\lvert F\rvert) = \sum_{\mathbf{H}} w(\mathbf{H})\,[\lvert F_o(\mathbf{H})\rvert - \lvert F_c(\mathbf{H})\rvert/K]^2. \quad (24)$$

Weights $w(\mathbf{H}) = 1$ were taken as this gives minimal fluctuations in difference maps $[\rho(\mathbf{r},\text{obs}) - \rho(\mathbf{r},\text{calc})]$ at the end of the refinement (Wilson, 1976; strictly speaking $w(\mathbf{H})$ = multiplicity of $\mathbf{H}$ should be taken). It should be noted, however, that in the present model calculations only $\frac{1}{3}$ of the reflections up to $\sin\theta/\lambda = 1{\cdot}2$ Å^{-1} is considered (§ 7.1). For $\alpha_1(\mathbf{H}) = 0$, the parameter differences

$$\Delta_i = p_i(\text{LS}) - p_i(\text{model}) \qquad (25)$$

should be zero. This was verified to be correct.

In all refinements anisotropic temperature factors were used and the full-matrix method was applied. For each C–H unit the differences in corresponding C and H parameters were kept equal to those in the model parameters. The number of independent parameters was thus reduced to 46. For all four sets of $|F_o(\mathbf{H})|$ values full angle (f.a.), low order (l.o.) and high order (h.o.) refinements were performed, where l.o. was chosen as $\sin\theta/\lambda < 0{\cdot}9$ Å^{-1} and h.o. as $\sin\theta/\lambda > 1{\cdot}0$ Å^{-1}, resulting in about 400 reflections in each range. For the refinements the *X-RAY* system (1973) was used.

Results

Table 6 summarizes the results of the refinements. It gives maximum and average parameter changes and the indices $R \equiv \{[\sum |F_o(\mathbf{H}) - F_c(\mathbf{H})/K|^2]/[\sum |F_o(\mathbf{H})|^2]\}^{1/2}$ before refinement, thus for $F_c(\mathbf{H}) = F_B(\text{model},\mathbf{H})$. During the refinements R dropped from the values given in the table to less than 0·6% in all cases. This indicates that the TDS contributions to the reflections are almost completely absorbed in the refined parameters.

(*a*) *Coordinates.* The Δ_i^{EX} values in Table 6 show that the errors in the coordinates due to TDS are very small. The largest value for the h.o. refinement is 7×10^{-4} Å and is approximately equal to the e.s.d.'s for accurate X-ray diffraction work at 100 K. Small changes of the same magnitude are found also by the LW, LWF and LWD methods.

(*b*) *Thermal parameters and scale factor.* The Δ_i^{EX} values in Tables 6 and 7 show that considerable errors occur in both the scale factor and the thermal parameters if no TDS corrections are made, and that these errors depend on the reflection range used in the refinement. Neglect of TDS corrections clearly gives too small values for the thermal parameters. For naphthalene at 100 K errors as large as 5×10^{-3} Å^2 are found, which is 10–15 times larger than the e.s.d.'s for accurate X-ray work. The fact that for each U_{ij} the average and maximum shifts are only slightly different, indicates that the errors are in good approximation equal for all atoms and thus occur in the translation tensors of the molecules. Table 6 shows that the change in this tensor is strongly anisotropic.

From Table 6 we see that first-order TDS calculations with the LW or LWF model tend to overcorrect the errors, but that good corrections can be made with the LWD method.

10. Use of TDS corrections for accurate X-ray work

The above discussion shows that accurate X-ray diffraction studies of naphthalene-type crystals at 100 K require TDS correction. This is especially true for accurate studies of bonding effects, in which high-order X-ray parameters or neutron diffraction parameters are used to calculate deformation maps including low-order reflections (Coppens, 1975). From Table 7 it is clear that high-order X-ray parameters are not transferable to the low-order region, if TDS corrections are neglected. It seems, however, that corrections at the LWD level are sufficient to eliminate the parameter

Table 6. *Results of the least-squares refinements*

The table gives the average and maximum values of Δ defined by (25) for the atomic positions (10^{-4} Å) and for the diagonal elements of the thermal vibration tensors (in 10^{-2} Å^2). ΔK is the shift in the scale factor in %, R is the one before refinement; R and K are defined in the text.

f.a. = full angle, l.o. = low order, h.o. = high order.

		LW			LWF			LWD			EX		
		f.a.	l.o.	h.o.	f.a.	l.o.	h.o.	f.a.	l.o.	h.o.	f.a.	l.o.	h.o.
$\lvert\Delta\mathbf{r}\rvert$	av.	3	3	3	8	8	5	2	2	1	2	2	4
	max.	5	5	5	9	12	9	3	3	2	4	3	7
$-\Delta U_{11}$	av.	0·52	0·56	0·40	0·52	0·56	0·41	0·40	0·43	0·32	0·40	0·43	0·32
	max.	0·54	0·57	0·41	0·54	0·57	0·41	0·41	0·43	0·32	0·42	0·43	0·33
$-\Delta U_{22}$	av.	0·20	0·21	0·15	0·19	0·20	0·15	0·20	0·21	0·16	0·20	0·21	0·15
	max.	0·20	0·21	0·15	0·20	0·22	0·15	0·20	0·21	0·16	0·21	0·21	0·16
$-\Delta U_{33}$	av.	0·14	0·15	0·09	0·14	0·14	0·09	0·13	0·13	0·09	0·13	0·14	0·09
	max.	0·15	0·15	0·09	0·15	0·16	0·10	0·13	0·14	0·09	0·13	0·14	0·10
ΔK (%)		1·0	0·7	6·1	1·0	0·7	5·8	0·7	0·4	4·6	0·7	0·4	4·6
R (%)		10·2	8·9	24·4	10·2	8·9	24·4	8·3	7·1	20·7	8·2	7·1	20·6

Table 7. *Comparison of the parameters obtained by low and high order least-squares refinement*

Given are $|\mathbf{r}(\text{LS,l.o.}) - \mathbf{r}(\text{LS,h.o.})|$, $U_{ii}(\text{LS,l.o.}) - U_{ii}(\text{LS,h.o.})$, and $K(\text{LS,l.o.}) - K(\text{LS,h.o.})$. Units as in Table 6.

		LW	LWD	EX
$\lvert\Delta\mathbf{r}\rvert$	av.	5	2	3
	max.	7	3	6
ΔU_{11}		−0·16	−0·11	−0·11
ΔU_{22}		−0·06	−0·06	−0·06
ΔU_{33}		−0·06	−0·04	−0·04
ΔK (%)		−5·4	−4·1	−4·2

errors due to first-order TDS and to make the errors in the individual reflections small (Table 5).

Compared with the EX method, the LWD method greatly reduces the computing time. Computing times on a Cyber 74-16 are 11 and 1 cpu s for EX and LWD respectively for the fixed scanned volume TDS calculations discussed above (for LW this time is 1 and for LWF 10).

11. Combination with experimental methods

The best way to reduce first-order and especially second-order TDS is to do the measurements at very low temperatures with a He cryostat. If TDS is reduced in that way, it may be hoped that theoretical interaction models are adequate to eliminate the remaining small TDS influence by making corrections in LWD, or even in LW, approximation. The LWF approximation is not considered further as it is no better than LW and requires much more computing time. Available computer programs will be modified so that first- and second-order TDS calculations can readily be done in LWD or in LW approximation for scanned volumes encountered in practice.

We thank the referee for valuable comments concerning second-order TDS and eigenvector dispersion. The computations were done at the Computing Center of the University of Groningen.

References

AFANAS'EVA, G. K. (1968). *Kristallografiya*, **13**, 1024–1027; *Soviet Phys. Crystallogr.* (1969), **13**, 892–895.

AFANAS'EVA, G., K., ALEKSANDROV, K. S. & KITAIGORODSKII, A. I. (1967). *Phys. Status Solidi*, **24**, K61–K65.

AFANAS'EVA, G. K. & MYASNIKOVA, R. M. (1970). *Kristallografiya*, **15**, 189–190; *Soviet Phys. Crystallogr.* (1971), **15**, 156–157.

ALEKSANDROV, K. S., BELIKOVA, G. S., RYZHENKOV, A. P., TESLENKO, V. R. & KITAIGORODSKII, A. I. (1963). *Kristallografiya*, **8**, 221–224; *Soviet Phys. Crystallogr.* (1964), **8**, 164–166.

BONADEO, H., MARZOCCHI, M. P., CASTELLUCCHI, E. & CALIFANO, S. (1972). *J. Chem. Phys.* **57**, 4299–4303.

BORN, M. & HUANG, K. (1968). *Dynamical Theory of Crystal Lattices*. Oxford: Clarendon Press.

CHANTRY, G. W., GEBBIE, H. A., LASSIER, B. & WYLLIE, G. (1967). *Nature (London)*, **214**, 163–165.

COCHRAN, W. (1963). *Rep. Prog. Phys.* **26**, 1–45.

COCHRAN, W. (1969). *Acta Cryst.* A**25**, 95–101.

COPPENS, P. (1975). *International Review of Science: Phys. Chem. Series* 2, Vol. 11, pp. 21–56.

CRUICKSHANK, D. W. J. (1957). *Acta Cryst.* **10**, 504–508.

FILIPPINI, G., GRAMACCIOLI, C. M., SIMONETTA, M. & SUFFRITTI, G. B. (1973). *J. Chem. Phys.* **59**, 5088–5101.

GRAMACCIOLI, C. M., SIMONETTA, M. & SUFFRITTI, G. B. (1973). *Chem. Phys. Lett.* **20**, 23–28.

HARADA, I. & SHIMANOUCHI, T. (1966). *J. Chem. Phys.* **44**, 2016–2028.

HARADA, I. & SHIMANOUCHI, T. (1967). *J. Chem. Phys.* **46**, 2708–2714.

HELMHOLDT, R. B. (1975). Thesis. Univ. of Groningen.

HELMHOLDT, R. B. & VOS, A. (1977). *Acta Cryst.* A**33**, 38–45.

HESELTINE, J. C. W., ELLIOTT, D. W. & WILSON, O. B. JR (1964). *J. Chem. Phys.* **40**, 2584–2587.

HOPPE, W. (1964). *Adv. Struct. Res. Diffr. Methods*, **1**, 90–166.

HUNTINGTON, H. B., GANGOLI, S. G. & MILLS, J. L. (1969). *J. Chem. Phys.* **50**, 3844–3849.

ITO, M., SUZUKI, M. & YOKOYAMA, T. (1968). In *Exitons, Magnons and Phonons in Molecular Crystals*, edited by A. B. ZAHLAN. Cambridge: University Press.

JAMES, R. W. (1965). *The Optical Principles of the Diffraction of X-rays*. London: Bell.

JENNINGS, L. D. (1970). *Acta Cryst.* A**26**, 613–622.

KROON, P. A. (1977). Thesis. Univ. of Groningen.

KROON, P. A. & VOS, A. (1978). *Acta Cryst.* A**34**, 823–824.

MARADUDIN, A. A., MONTROLL, E. W. & WEISS, G. H. (1963). *Theory of Lattice Dynamics in the Harmonic Approximation. Solid State Phys. suppl.* 3.

MIRSKAYA, K. V., KOZLOVA, I. E. & BEREZNITSKAYA, V. F. (1974). *Phys. Status Solidi B*, **62**, 291–294.

PAWLEY, G. S. (1967). *Phys. Status Solidi*, **20**, 347–360.

PAWLEY, G. S. (1972). *Phys. Status Solidi B*, **49**, 475–488.

PAWLEY, G. S. & CYVIN, S. J. (1970). *J. Chem. Phys.* **52**, 4073–4077.

REID, J. S. (1973). *Acta Cryst.* A**29**, 248–251.

SCHERINGER, C. (1973*a*). *Acta Cryst.* A**29**, 283–290.

SCHERINGER, C. (1973*b*). *Acta Cryst.* A**29**, 554–570.

STEVENS, E. D. (1974). *Acta Cryst.* A**30**, 184–189.

TADDEI, G., BONADEO, H., MARZOCCHI, M. P. & CALIFANO, S. (1973). *J. Chem. Phys.* **58**, 966–978.

TESLENKO, V. F. (1967). *Kristallografiya*, **12**, 1082–1084; *Soviet Phys. Crystallogr.* (1968), **12**, 946–948.

WALKER, C. B. & CHIPMAN, D. R. (1970). *Acta Cryst.* A**26**, 447–455.

WILLIAMS, D. E. (1966). *J. Chem. Phys.* **45**, 3770–3778.

WILLIAMS, D. E. (1967). *J. Chem. Phys.* **47**, 4680–4684.

WILLIAMS, D. E. (1970). *Trans. Am. Crystallogr. Assoc.* **6**, 21–33.

WILLIAMS, D. E. (1974). *Acta Cryst.* A**30**, 71–77.

WILLIS, B. T. M. (1969). *Acta Cryst.* A**25**, 277–300.

WILSON, A. J. C. (1976). *Acta Cryst.* A**32**, 781–783.

X-RAY system (1973). Dutch version. Technical Report TR-192 of the Computer Science Centre, Univ. of Maryland. June, 1972.